Running Title: Protein-based traits in *Synechococcus*

Title: Proteome trait regulation of marine *Synechococcus* elemental stoichiometry under global change

Nathan S Garcia[1,*], Mingyu Du[2], Michele Guindani[2], Matt R McIlvin[3], Dawn M Moran[3], Mak A Saito[3], and Adam C Martiny[1,4]

[1] 3200 Croul Hall, Department of Earth System Science, University of California, Irvine, CA 92697, USA

[2]Department of Statistics, University of California, Irvine, CA 92697, USA

[3] Marine Chemistry and Geochemistry Department, Woods Hole Oceanographic Institution, Woods Hole, MA 02543, USA

[4]Department of Ecology and Evolutionary Biology, University of California, Irvine, CA 92697, USA

*Corresponding author: n8garcia@gmail.com

Abstract

Recent studies have demonstrated regional differences in marine ecosystem C:N:P with implications for carbon and nutrient cycles. Due to strong co-variance, temperature and nutrient stress explain variability in C:N:P equally well. A reductionistic approach can link changes in individual environmental drivers with changes in biochemical traits and cell C:N:P. Thus, we quantified effects of temperature and nutrient stress on *Synechococcus* chemistry using laboratory

chemostats, chemical analyses, and data-independent-acquisition mass-spectrometry proteomics. Nutrient supply accounted for most $C{:}N{:}P_{cell}$ variability and induced tradeoffs between nutrient acquisition and ribosomal proteins. High temperature prompted heat-shock, whereas thermal effects via the 'translation-compensation hypothesis' was only seen under P-stress. A Nonparametric Bayesian Local Clustering algorithm suggested that changes in lipopolysaccharides, peptidoglycans, and C-rich compatible solutes may also contribute to C:N:P regulation. Physiological responses match field-based trends in ecosystem stoichiometry and suggest a hierarchical environmental regulation of current and future ocean C:N:P.

Keywords: *Synechococcus*, nutrient stress, temperature stress, resource allocation, elemental stoichiometry, proteome, traits, growth rate hypothesis, global change

Introduction

The relative composition of elements in phytoplankton (i.e., C:N:P) is central to ocean functioning. This includes environmental interactions with biodiversity[1], ecological and trophic exchanges[2, 3], nitrogen fixation[4], and the biological pump[5]. The C:N:P composition of ocean phytoplankton has been assumed constant for many decades – i.e., the Redfield Ratio of 106:16:1[6]. Although field studies now demonstrate strong regional and temporal variation in elemental stoichiometry of marine communities[7–9], the underlying controls of ocean C:N:P are not well-constrained. A trait-based approach can provide a mechanistic biochemical understanding of C:N:P regulation and improve modeled ecosystem responses to global change.

Several biochemical mechanisms are thought to control phytoplankton elemental ratios[10, 11], but are difficult to identify due to multiple influential factors. The most prominent hypotheses involve element storage and regulation of P-rich ribosomes - the machinery for biosynthesis. The nutrient supply theory posits that cells are frugal under nutrient scarcity but increase storage when nutrients are abundant[12–16]. This mechanism can result in a correspondence between nutrient concentrations and $C{:}N{:}P_{cell}$[5]. The translation compensation hypothesis posits that P-rich ribosomes are abundant at low temperature to compensate for slow translational activity, leading to depressed C:P and N:P ratios in high-latitude ecosystems[17, 18]. Finally, the growth rate hypothesis posits that cellular growth also has specific requirements for ribosomes that can directly affect $C{:}N{:}P_{cell}$, resulting in tradeoffs with other cellular components[19, 20]. The challenge is that each of these biochemical mechanisms can explain current field observations equally well due to latitudinal co-variance between nutrient stress, temperature, and growth status of phytoplankton. Controlled laboratory experiments, mimicking balanced growth conditions in the oceans, provide a way to distinguish environmental effects on specific traits and elemental allocations.

Biomolecular studies suggest that phytoplankton employ several additional mechanisms to manage environmental stress. For example, nutrient stress influences N-rich nutrient acquisition proteins[21] and phycobilisomes[22]. Sulfolipids can replace phospholipids in membranes of Cyanobacteria under P-stress[23–25], thereby reducing the P quota. Polyphosphates (poly-P) can store P[16], but also serve a variety of physiological functions[26, 27]. More recently, the periplasm was suggested as a nutrient docking and storage site that assists in cell nourishment[15]. However, the contribution of these molecular mechanisms to cellular elemental stoichiometry is unclear[10], particularly under balanced growth, and we have a limited view of the contribution of each biochemical mechanism and associated traits to the regulation of *C:N:P* in the field.

Here, we quantified the relative impacts of temperature and nutrient stress on cellular C:N:P in one of the largest contributors to ocean primary production, *Synechococcus*[28]. To account for growth rate effects, we normalized to continuous growth with a chemostat culture design. To understand the trait-based biochemical regulation of cell quotas, we integrated analyses of cellular elemental resource allocations with data-independent acquisition mass spectrometry (DIA-MS) proteomics. Combined, these analyses provide a molecular view of trait regulation of C:N:P in an abundant marine phytoplankton.

Methods

Experimental design and elemental analysis

We grew *Synechococcus* cultures (WH8102) in polycarbonate bottles with a continuous method used previously[29] in artificial seawater (Table S1). We used two concentration ratios of macronutrients (NO_3^-:PO_4^{3-} = 1.7 and 80) and 3 levels of temperature (20, 24 and 28°C) with a slow dilution rate to ensure treatment-wise culture stability. White light was supplied at 125

μmol quanta m^{-2} s^{-1} on a 12h:12h light:dark cycle. Equilibria were monitored by measuring culture cell density and forward scatter (FSC_H) with a Novocyte flow cytometer 1000 (Acea Biosciences, Inc, San Diego, CA). Biomass was collected after an acclimation period on days 38, 43, 47, 50 and 57 for particulate organic matter, nutrient analysis, cellular proteins, culture cell density and FSC_H (Figure S1). Particulate organic carbon and nitrogen (150 mL) and phosphorus (50 mL) were collected at the midpoint of the light period with glass fiber filters (GF/F, Whatman, GE Healthcare, Little Chalfont, Buckinghamshire, UK) and measured using a Flash EA1112 gas chromatograph (Thermo Scientific) and a Genesys 10S UV-vis spectrophotometer (Thermo Scientific, Madison, WI, USA) at 885 nm following methods described by Michaels et al.[30]. Culture cell density and FSC_H were measured in samples collected for biomass. Cells for proteome analysis were collected with a 47 mm polycarbonate filter (0.2 μm pore size) 7-8 hours into the light period, pelleted by centrifugation (21,130 g for 3 minutes), flash frozen in liquid nitrogen and stored at -80°C.

Protein extraction and peptide preparation

Proteins were extracted by heating pelleted cells at 95˚C for 10 min and gently shaking at room temperature for 30 min in a buffer solution (400 μL – 1760 μL; 50 mM HEPES pH 8.5 (Boston BioProducts #BB-2082), 1% SDS in HPLC grade water) before centrifuging at 14100 g for 20 min at room temperature and removing the supernatant. Sodium dodecyl sulfate (1%) is a strong detergent for diverse matrices including cell membranes[31]. Benzonase nuclease (50 units; Novagen #70746-3) was added to 400 μL extracted protein sample and incubated at 37˚C for 30 min. Samples were reduced by adding 20 μL of 200 mM DTT (Fisher #BP172-5) in 50 mM HEPES pH 8.5 at 45˚C for 30 min and alkylated with 40 μL of 400 mM iodoacetamide

(Acros #122270050) in HEPES pH 8.5 for 30 min at 24˚C. The reaction was quenched by adding 40 µL of 200 mM DTT in 50 mM HEPES pH 8.5. SpeedBead Magnetic Carboxylate Modified Particles (GE Healthcare #65152105050250 and #45152105050250) were prepared according to[31] and added (20 µg/µL) to 400 µL of extracted protein sample. Samples were incubated with formic acid (pH of 2-3) and washed with ethanol and acetonitrile using a magnetic rack. Protein was measured with the BCA method (Thermo Scientific Micro BCA Protein Assay Kit #23235) and digested overnight at 37˚C with 1 part trypsin (Promega #V5280; dissolved in HEPES pH 8.0, 0.5 µg/µL), 25 parts protein. Peptides were washed with acetonitrile and ethanol using a magnetic rack and diluted to a target concentration of 0.1% trifluoroacetic acid or 1% formic acid and a final concentration of 1 µg/µL.

Mass spectrometry of peptides

Similar to other analyses[32], peptides were analyzed using a Michrom Advance HPLC system coupled to a Q-Exactive mass spectrometer (Thermo Scientific instrument version 2.8) with a Michrom Advance CaptiveSpray source, using the constant injection concentration of 1 µg/µL to allow uniformity across the dataset. Samples were concentrated onto a C18 column (Reprosil-Gold, Dr. Maisch GmbH) and eluted in a non-linear, 200-min gradient of formic acid and acetonitrile buffers. Full MS1 scans were performed (35,000 resolution, 3e6 AGC target, 60 ms maximum IT, 385 to 1015 m/z) with overlapping DIA scans (17,500 resolution, 1e6 AGC target, 60 ms maximum IT, 24.0 m/z isolation windows, normalized collision energy of 27, loop count 25, see supplementary material for expanded methods).

Proteomic data analysis

DIA-MS sample data were analyzed using Scaffold DIA (2.2.1), converted to mzML format (ProteoWizard 3.0.11748) and individually searched against Syn8102_uniprot-proteome_UP000001422.fasta with a peptide and fragment mass tolerance of 10.0 ppm. Percolator (3.01) filtered peptides for a maximum false discovery rate of 0.01. Charged peptides (2-3) with length (6-30) were considered. EncyclopeDIA (0.9.6) selected the 5 highest quality fragment ions for quantitation[32]. Within the total proteome, 1215 proteins were identified with 2 or more representative peptides. However, we only included 1146 proteins in the broader analysis since some of the proteins were not detected across the entire sample set. Thus, we removed proteins that returned a "missing value" in 3 or more of the samples (10% or more), keeping only those returning 2 or less missing values across the 30-sample set. Mean total peptide peak areas were normalized across all samples with the Scaffold DIA Proteome Software to allow intercomparisons across samples (Proteome Software, Inc., Portland, OR; Supplementary Figure S2). We summed peak areas of peptides assigned to all observable proteins in our calculation of relative protein abundances. We then analyzed treatment effects on the relative sum of peak areas of proteins within specific groups related to phycobilisomes, N- and P-acquisition, biosynthesis, heat shock, cell motility, photic electron transport, oxidative stress, cell structure, metals transport and CO_2 fixation (identifying references[33–36], see TS7 for protein group identification). We compared *PA* of a protein or protein group to the PA_{Total} for each sample (n=5 for each treatment) and report statistics for treatments.

$$\% PA_{Total} = protein\ or\ protein\ group\ PA\ /\ PA_{Total}\ x\ 100$$

We interpret these summed peak areas of tryptic peptides as reflective of cellular resources being deployed for each function, rather than of copy number since proteins have lengths and numbers of peptides. Moreover, while there are differences in ionization efficiency between peptides, the summed peak areas provided an aggregate metric to consider allocation of cellular resources within protein groups. Assumptions within data preparation had a very minor impact on results: the use of a more stringent 2 peptides per protein caused a loss of only 0.34% of total peak area, and removal of proteins missing in more than two samples resulted in loss of 0.33% total peak area (Supplementary Table S2). We also considered a group that includes 100 proteins with the highest mean *PA*, which accounted for 74±SE 2.5% of PA_{Total} (Supplementary Figure S2) indicating that less than 10% of the observable proteins contribute to a large majority of the protein mass. The mass spectrometry proteomics data have been deposited to the ProteomeXchange Consortium via PRIDE [1] partner repository with the dataset identifier PXD043180.

Analysis of variance and clustering analyses

We relied on the 2-way Analysis of Variance to describe differences in cellular elemental quotas and ratios and FSC_H of *Synechococcus* using the *anova2* function in Matlab (The Mathworks, Inc.). To describe variability in proteins, we relied on a variety of methods including the 2-way Analysis of Variance, Benjamini-Hochberg pairwise comparisons test, Permutational Multivariate Analysis of Variance on protein groups using the *adonis2* function from the *vegan* package in *R*, a hierchichal clustergram function for protein analysis in Matlab, and a Nonparametric Bayesian Local Clustering (NoB-LoC) algorithm.

We fit the NoB-LoC algorithm to 1146 proteins[37]. This method uses the Dirichlet process mixture model with the zero-enriched Pólya urn scheme[38] and partitions proteins into sets or biclusters that have similar distributions of relative abundance within sub-partitions or subclusters, regardless of mean value (e.g. low vs. high relative abundance), thereby classifying proteins based on response patterns. To reduce stringency on biclusters the method identifies "invariant" proteins and samples that do not follow broader distribution patterns within identified subcluster distributions.

We initialized the biclustering indicator ω by removing non-clustering proteins (singletons) from hierarchical clustering and designated them as "invariant", meaning they do not follow distribution patterns that are similar to other proteins. There are 20 variant protein sets and 1 invariant set including 10 proteins in the initialized partition of our model. Moreover, in order to incorporate biological information that most biological processes involve only a small subset of proteins, we set up a prior construction of ω by assuming that a protein g is invariant ($\omega_g = 0$) with probability $(1 - \pi_0)$, where ω_g is the cluster membership indicator for protein g. Here we set $\pi_0 = 0.01$, which allows a small subset of proteins to be involved in a pathway. We implemented a Markov Chain Monte Carlo (MCMC) simulation with 35,000 iterations with 5,000 burn-in iterations. To measure the uncertainty of estimation, we used a distance metric

$$H(\omega, \omega^{LS}) = \sum_{g=1}^{G} \sum_{g\prime=g}^{G} \left| d_{g,g\prime}^{\omega} - d_{g,g\prime}^{\omega^{LS}} \right|$$

in which, $d_{g,g\prime}^{\omega} = I(\omega_g = \omega_{g\prime})$ is an indicator of whether the protein g and g' are clustered together in partition ω and $d_{g,g\prime}^{\omega^{LS}}$ is the clustering indicator for the estimated partition ω^{LS}. The posterior distribution of scaled distance metric for ω is reasonable with low variability around zero (Supplementary Figure S3).

We identified 8 biclusters and 317 invariant proteins with this method. To identify relative partitioning of proteins into biclusters we ranked them by % PA_{Total} (Supplementary Figure S3). We then used the proportional difference from the mean log peak area of a given protein (mean calculated across all 30 samples) and arranged proteins in order based on the proportional difference from mean values to identify proteins with similar responses to nutrients and temperature stress (Supplementary Table S3).

Results

Changes in cellular elements and cell size

To quantify molecular trait regulation of *Synechococcus* elemental composition, we used a factorial chemostat design to grow WH8102 under a range of temperature and nutrient stress levels. The two-factorial design covered P-stress ($N{:}P_{input}$ = 80:1) and N-stress ($N{:}P_{input}$ = 1.7:1) at 20˚C, 24˚C and 28˚C. We measured our fixed dilution rate across treatments at 0.178±0.004(mean±SD) d^{-1}, which we controlled to isolate effects of nutrient and temperature stress from growth rate effects on cellular biochemical regulation. Specifically, we measured equilibrium cellular C-, N- and P-quotas, FSC_H (cell size proxy) using flow cytometry, and relative protein abundances using data-independent-acquisition mass spectrometry proteomics.

Cell size was smallest at 24˚C and largest at 28˚C (Figure S4E) and changes in elemental quotas were linked to FSC_H, reducing variability in $Q{:}FSC_H$ (Figure 1D,E,F, S4E, TS4). Element-use efficiency for growth (i.e. the material needed to achieve a given cell replication rate) peaked at 24˚C, thereby defining the optimal temperature (T_{opt}) for element-use. Although mean Q_N was slightly elevated under P-stress at 20-24˚C, $Q_N{:}FSC_H$ was relatively invariable across treatments (Figure 1E, Table S4E), indicating that elevated N quotas under P-stress

resulted from larger cells rather than increased N-density. However, we observed two deviations from the elemental quotas vs. cell size coupling. First, Q_C:FSC_H was elevated at low to mid temperature in N-stressed cells indicating that cells were more carbon-dense relative to other treatments (Figure 1D). Second, Q_P:FSC_H was nearly 3-fold higher under N- vs. P-stress and slightly higher at low temperature relative to T_{opt}, but only under P-stress (Figure 1F). Thus, cell size and Q are key links to understand environmental regulation of cellular elements.

We identified a clear hierarchical environmental effect on cellular elemental ratios. $N:P_{input}$ accounted for 93 and 95% of total $C:P_{cell}$ and $N:P_{cell}$ variances, respectively (Figure 2), and $C:P_{cell}$ and $N:P_{cell}$ more than doubled when shifting from N- to P-stress (Figure 1G-H). Nutrient stress effects on $C:P_{cell}$ and $N:P_{cell}$ were driven by cellular P-savings, (e.g. 36% reduction of Q_P under P-stress at 24°C, TS4). Nutrient stress also impacted $C:N_{cell}$ (61% of variance), but the effect size was smaller (Figure 2). $C:N_{cell}$ was only 5-19% higher under N- relative to P-stress (Figure 1I), linked to differences in Q_C rather than N-density (Figure 1D-E). Temperature explained less variance overall with 1-2% for $C:P_{cell}$ or $N:P_{cell}$ and 10% for $C:N_{cell}$ (Figure 2). However, corroborating the translation compensation hypothesis, temperature positively affected $C:P_{cell}$ under P-stress but not N-stress, resulting in a 17% increase between 20˚C and 28˚C (Figure 1G). This suggested nutrient stress and temperature interact to influence $C:P_{cell}$. Likewise, nutrient stress and temperature also interacted on $C:N_{cell}$, where the $N:P_{input}$ effect decreased with rising temperature (Figure 1I). In summary, nutrient stress had a primary and temperature a secondary effect on cellular elemental stoichiometry.

Changes in protein-based traits

Key cellular traits varied significantly with nutrient and temperature stress. The 1146 proteins in our analysis represent >99% of the total peak area of the 1425 proteins that we

240 detected (Table S2), which includes 57% of the 2512 protein-coding genes in WH8102. A 2-way
241 PERMANOVA analysis indicated that $N{:}P_{input}$ accounted for 54% of the proteome variance
242 (Figure 2, Table S6). Nutrient-acquisition proteins formed the most frequent trait and responded
243 strongly to changes in $N{:}P_{input}$ (Figures 3 and 4). Under P-stress, the possible porin (SomB,
244 Q7U448), phosphate-binding protein (PstS, Q7U7G6) and alkaline phosphatases (n=4, including
245 two phytase-like proteins identified in P-blast, Q7U9T8 & Q7U862) had the largest peak area
246 (Figures 3 and 4). When treatment means of % PA_{Total} were averaged over temperature
247 treatments (as in Table TS7), allocation to P-acquisition constituted between 14% and 20% of
248 the total proteome under P-stress (Figure 4B; Figure S5; Table S7). Under N stress, N-
249 acquisition proteins were also induced but did not require the same high protein investment as P-
250 acquisition (Figure 4B-C). The induced N-acquisition proteins included another possible porin
251 (Som, Q7U447) along with nitrate, nitrite, cyanate, and urea assimilation proteins. Iron and zinc
252 acquisition proteins were also more frequent under N-stress suggesting an increased demand for
253 metal co-factors for nitrate reduction and other N-acquisition mechanisms (Figure 4J). When
254 summed, all nutrient acquisition proteins (P-acquisition, N-acquisition and metal transport)
255 represented 5-7% more of the total proteome under P-stress relative to N-stress (Figure 4B-C and
256 J; Table S7), thereby accounting for a portion of the elevated Q_N under P-stress. Ribosomal
257 proteins ranged from 3.3-7.7% of PA_{Total} and also varied as a function of $N{:}P_{input}$ (Figure 4D;
258 Table S7). Within temperature treatments, relative ribosomal protein abundances were 37-40%
259 lower under P- vs. N-stress, with reduced contributions to PA_{Total} by 2-3% (Figure 4D). Thus, P-
260 stress resulted in the largest increase in a single trait (all nutrient acquisition proteins - *NAP*,
261 Figure S4F) and the largest decrease in P-rich ribosomal proteins. To illustrate this influence on
262 $C{:}P_{cell}$ stoichiometry, we compared the ratio of *NAP* to calculated estimates of rRNA and

identified a major correspondence between nutrient-wise changes in $C:P_{cell}$ and ratios of *NAP:rRNA* investments (Figure S4H). Overall, the proteome responded dynamically, with *NAP* and ribosomal proteins representing the strongest responses to nutrient stress.

Temperature had an additional albeit weaker influence on the proteome and accounted for 2.8% of the variance (Figure 2). The heat-stress proteins, dominated by the chaperonins and co-chaperonins (GroES, GroELS, DnaK2), increased in relative abundance from 20˚C to 28˚C. As a result, the heat stress trait comprised ~10% of the total proteome at 28°C (Figure 4E). This trait responded orthogonally with the biosynthesis trait. As temperature increased from 20 to 24˚C, relative ribosomal protein abundances declined by 29% under N-stress and 24% under P-stress (Figure 4D). Only minor declines were seen when shifting to 28˚C. Similarly, protein allocations for photosynthetic electron transport and ATP synthesis also decreased with increasing temperature suggesting a wider thermal effect on core metabolic functions (Figure 4D, TS7 and TS8). Furthermore, our analysis identified interactive relationships between temperature and nutrients on multiple biochemical functions. These functions included ATPases, phycobiliproteins, the oxidative pentose phosphate (PP) pathway, and enzymes involved in cell structure (Figure 4; Figure S6; Tables S6-S8). While N-stress and temperature had a positive interactive effect on relative abundances of phycobiliproteins (Figure 4A; Tables S6-S8), P-stress and temperature had a positive interactive effect on relative abundances of glucose-6-phosphate dehydrogenase and OpcA that support the oxidative PP pathway (Figure S6)[39, 40]. The oxidative PP pathway supplies NADPH, a process commonly associated with the dark cycle in Cyanobacteria[41], but here, was favored in the middle of the light period under P-stress relative to N-stress. Overall, thermal influences included a robust positive effect on heat-shock proteins

across nutrient treatments, compensatory responses with declining temperature, and interactive effects with nutrients on processes involved in relative carbon accumulation and use.

Changes in central metabolism

We next applied a Nonparametric Bayesian Local Clustering algorithm to explore how shifts in central metabolism could influence cellular elemental allocations. Our analysis highlighted shifting carbon metabolism, compounds involved in osmotic regulation, cell wall biosynthesis, and poly-P accumulation as additional traits affecting cell quotas. First, several proteins involved in glycogen utilization were more abundant under P- relative to N-stress (Figure S6). While the glycogen synthesis enzyme, 1,4-alpha-glucan branching enzyme (GlgB, Q7U646, bicluster 4) was only slightly induced under N-stress relative to P-stress at 20˚C, other glycogen synthesis enzymes including glycogen synthase (GlgA, Q7U7I2, bicluster 7) and glucose-1-phosphate adenylyltransferase (GlgC, Q7U768, bicluster 5) were stable between temperature treatments (Figure S6), indicative of weak support for upregulated glycogen synthesis pathways under N-stress. Instead, the glycogen digestive enzyme α−1-4 glucan phosphorylase was more frequent under P-stress and glycosyl hydrolase (Q7U4W1, bicluster 8), a versatile enzyme class that may also be involved with sugar degradation, also clustered with several established P-stress proteins regardless of temperature (Table S3). Combined, relative changes in abundances of these digestive enzymes suggested elevated organic carbon use and therefore less accumulation under P-stress (Supplementary Figure S6). While we did not measure glycogen concentrations directly, the results align well with the reduced Q_C:FSC_H under P-stress. Second, expression of glucosyl-3-phosphoglycerate synthase (Q7U3J6) clustered with relative abundances of several proteins clearly involved in N-stress (Table S3, bicluster 5). Glucosyl-3-phosphoglycerate synthase supports replacement of glutamate with the N-free, C-rich

compatible solute glycosyl-glycerate (GGA) under N-stress in *Synechococcus*[42, 43]. This result aligns with the increased Q_C:FSC_H under N-stress and comparative calculations of GGA align with observed C:N variability (Table TS11). Third, we observed a putative P-stress-dependent regulation of precursors to peptidoglycan and lipopolysaccharides (LPS). These pathways including N-acetyl-glucosamine-6-phosphate deacetylase (NagA, Q7U3Z1, bicluster 8), N-acetylmuramic acid 6-phosphate etherase (MurQ, Q7U6S0, bicluster 3), and the bifunctional protein for UDP-N-acetylglucosamine (GlmU, Q7U710, bicluster 3)[44, 45], are involved with metabolism of either cell wall or membrane components and clustered with several P-acquisition proteins (replotted in Figure S6; Table S3). Collectively, this suggests that the biosynthesis pathway to UDP-N-acetylglucosamine and the placement of this monomer in either peptidoglycan or LPS is more active under P-stress relative to N-stress. Elevated cell concentrations of peptidoglycans and N-enriched, cross-linked oligopeptides under P-stress align with elevated N-quotas. Fourth, our calculations indicate that temperature had a positive influence on the portion of Q_P that is apportioned to cell components other than nucleic acids (Figure S4B) and on enzymes controlling the synthesis vs. degradation of polyphosphate (Figure S4C-D). In sum, we observed nutrient- and temperature-stress effects on key metabolic pathways that are involved in cellular use of carbon, nitrogen and phosphorus.

Discussion

Existing hypothesis for biochemical regulation of C:N:P_{cell}

We found mixed support for existing hypotheses describing elemental allocation in *Synechococcus*[11]. Elemental quotas, ratios and FSC_H at 24°C aligned with previous data from chemostat cultures of WH8102 [29] and supported the nutrient supply hypothesis for $C{:}P_{cell}$ and

331 $N{:}P_{cell}$, mostly through differences in the P-quota. However, $N{:}P_{input}$ interacted with temperature
332 to affect $C{:}N{:}P_{cell}$ through the thermal influence on ribosomes that may have arisen from the
333 translation compensation mechanism. We interpret this interactive environmental effect as driven
334 by high P-quotas under N-stress, which overwhelms a small thermal effect on ribosomes and
335 associated P-requirements. This interpretation is partially supported by the large $N{:}P_{input}$ effect
336 on ribosomal proteins, which contributes to the large nutrient-wise effect on $Q_P{:}FSC_H$. Thus,
337 ribosomes add to a list of biochemicals, such as phospholipids[46], phosphorylated
338 phycobiliproteins[47], polyphosphates[16] and P-storage[15] that can harbor P under P-replete
339 conditions. To estimate allocations amongst P-pools, we rely on other data[25] to calculate that
340 P-savings from sulfolipid replacement in WH8102 only reduced Q_P by 2%, similar to measured
341 estimates [46]. However, rRNA and unidentified pools reduced Q_P by 10% and 24%,
342 respectively, at 24°C. In support of a previous hypotheses regarding nutrient-acquisition
343 proteins[21, 48], P-acquisition proteins along with N in peptidoglycans can account for a portion
344 of the increase in Q_N and FSC_H under P-stress. As Q_C and Q_N are linked through proteins and
345 peptidoglycans, high relative abundances of these integral membrane/wall structures may be
346 important traits that contribute to cell size and elemental ratios. In sum, the translation
347 compensation mechanism may have impacted $Q_P{:}FSC_H$ and $C{:}P_{cell}$ under P-stress but not N-
348 stress due to the overwhelming $N{:}P_{input}$ effect on $Q_P{:}FSC_H$. The $N{:}P_{input}$ effect was also large but
349 opposite in sign on *NAP*. These opposing effects on ribosomes and *NAP* combined to amplify
350 nutrient-wise differences in $C{:}P_{cell}$ and $N{:}P_{cell}$. Because chemostat dilution rates are similar to
351 implied rates in ocean gyres[49], our interpretations are likely applicable to field data.
352
353 *New and alternate hypotheses for biochemical regulation of* $C{:}N{:}P_{cell}$

Our proteomics analysis allowed for new perspectives of biochemical regulation of $C:N:P_{cell}$. First, nutrient regulation of $C:N_{cell}$ was not strong but was interactive with temperature. As hypothesized from Droop-like models[19], we detected higher $C:N_{cell}$ under N-stress relative to P-stress, but not at high temperature. In contrast to other data that identify large variability in Q_N as a function of $N:P_{input}$[46, 50], $Q_N:FSC_H$ was nearly constant between treatments. Instead, changes in $C:N_{cell}$ were driven by $Q_C:FSC_H$. Multiple studies have identified broad correspondence between cell volume and carbon biomass but have also identified considerable variability within a size class and associated variation in cellular carbon density[51, 52]. Our data suggest at least two pathways for size-independent increases in cellular carbon density under N- compared to P-stress. First, P-stress induced multiple pathways for carbon respiration, whereas N-stress induced only minor support for elevated glycogen production. Second, N-stress supported high glucosyl-3-phosphoglycerate synthase abundance, the enzyme responsible for replacing N-rich glutamate with the C-rich compatible solute GGA[43], and our hypothetical calculations of $C:N_{cell}$ with GGA replacement support previous data regarding GGA in Cyanobacteria[43, 53]. Third, the interactive treatment effect on $C:N_{cell}$ may include N-rich phycoerythrin since relative abundances increased with temperature under N-stress and not P-stress. This result is different than past observations of degraded phycobiliproteins under N-stress[22] but has been observed in a mutant strain of *Synechococcus* devoid of a glycogen synthesis enzyme[54], a condition similar to the weak support for an N-stressed glycogen synthesis process that we observed in WH8102. Instead, phycobiliproteins may protect cells, perhaps through state transitions[55], in acclimated, slow-growing cells. Overall, our proteomic results suggest a more complex regulation of $C:N_{cell}$ in marine phytoplankton than previously recognized.

Next, although we identified biochemical support for the translation compensation hypothesis, the temperature effect on Q_P:FSC_H was small between 20-28°C and other hypotheses may be more important for Q_P dynamics and marine ecosystems within this thermal range. As hypothesized, we observed a negative relationship between temperature and ribosomal proteins[11, 17]. However, the thermal effect on ribosomal proteins and $C:P_{cell}$ only seems observable under P-stress, when other P-resources, like polyphosphates or periplasm-P are minimized or depleted. By comparison the nutrient-wise effect on ribosomal proteins was large, a trend supported in previous studies of *Synechococcus* WH8102[29, 56]. Elevated ribosome abundances under P-repletion may scavenge P at an N-cost in non-active ribosomes[55]. Alternatively, streamlined efficiency[57] of ribosomes under P-stress could result from high production of abundant proteins like PstS and alkaline phosphatases. In either case, P-supply has opposing effects on Q_{CN} and Q_P through *NAP* and ribosomes, respectively, that together contribute to large changes in $C:P_{cell}$ and $N:P_{cell}$. Because this efficiency ratio of *NAP*:ribosomes peaked at 24°C (supporting other estimates of T_{opt} for WH8102[58]), along with cell carrying capacity (Figure S1A), and elevated protein chaperone abundances suggest thermal stress at 28°C [33, 59, 60], this efficiency mechanism may be important for *Synechococcus* ecology. For example, the cell-shape-determining protein MreB[61] or cell division metrics[62] may be important regulators of microdiversity because of inherent links between cell size, T_{opt} for element-use efficiency and carrying capacity.

There are caveats for linking our experiments with large-scale regulation of C:N:P. First, our investigation using DIA-MS proteomics approaches a comprehensive analysis but future investigations of biodiversity in cellular P dynamics will help to delineate Q_P regulation. Second, our analysis of % PA_{Total} approximates relative protein investments into specific traits rather than

relative comparisons of protein copy numbers between treatments. Third, due to the complexity of chemostat experiments, we only examined a single strain under limited environmental conditions. However, variability in the field includes broader conditions and more diverse phytoplankton lineages. For example, %P-savings from sulfolipid replacement are variable between strains of *Synechococcus*[25]. Fourth, our definition of T_{opt} for element-use efficiency is different than the definition of T_{opt} for growth rate and seems more relevant under nutrient limitation. Fifth, our proteome analysis excludes proteins that are not well-represented or absent across treatments. Despite these caveats, our molecular information helps constrain the regulation of phytoplankton biochemistry. Exploring more lineages, environmental conditions, and biochemical assays will improve our understanding ocean C:N:P.

Implications for field observations

Field observations indicate that nutrient stress drives C:N:P in low-latitude ecosystems, where the thermal effect is relatively small[9]. Similarly, temperature had little effect on $C{:}P_{cell}$ and $N{:}P_{cell}$ in our cultures under N stress - the most frequent nutritional condition observed across oceans[63]. However, ecosystem observations do indicate that C:P and N:P is slightly depressed at high temperature, possibly due to heat-stress[9]. Conversely, in high-latitude, cold ecosystems, temperature shifts play a stronger role in driving C:N:P variability compared to the thermal range in our design[9, 17]. The relatively weak influence of temperature on $C{:}N{:}P_{cell}$ observed here implies that lineage-wise variability in C:N:P or thermal influences in other lineages are stronger in the field. Thus, shifts in biodiversity may contribute to C:N:P variability in the surface ocean beyond the physiological mechanisms described here. Hence, the combined

422 field and experimental data suggest complex effects on C:N:P in marine ecosystems that
423 incorporate current hypotheses and evolving theories.
424
425 **Acknowledgements**
426 We thank Alyse Larkin and Renne Harcourt for assistance with lab work and Juhee Lee and
427 colleagues for the statistical clustering computer code. This study was supported by NSF grant
428 OCE-184857680 and OCE-2135035 to A.C.M, IOS-2137339 to N.S.G. and A.C.M., UCI ICS
429 Exploration Award to M.G., and Simons Foundation and NSF grant to M.A.S.

Data Availability

Cell data are accessible in the Supplementary Table S4. Proteomics data are available via ProteomeXchange (PXD043180). For reviewer purposes the data can be accessed with:

Username: reviewer_pxd043180@ebi.ac.uk

Password: xWseA7Fk

Codes and instructions for implementing the Nonparametric Bayesian Local Clustering algorithm on proteomics are available on GitHub at https://github.com/mingyudu/NoB-LoC.

Competing Interests

The authors declare no competing interests.

Figure Legends

Figure 1. **Relative influence of nutrient supply and temperature on cellular elemental quotas and ratios of marine *Synechococcus* (WH8102)**. A) Carbon cell quota (fmol cell^{-1}) B) nitrogen cell quota (fmol cell^{-1}) C) phosphorus cell quota (fmol cell^{-1}), D-F) Means with standard deviations (n=5) of cell quotas normalized to size proxy (forward scatter, FSC_H), G) C:P, H) N:P and I) C:N cellular elemental ratios (mol/mol). Cultures were grown at 20, 24, and 28°C and diluted at 0.18 d^{-1} with a nitrate:phosphate input ratio of 80 (blue symbols, P-stressed) and 1.7 (dark red symbols, N-stressed). Data between nutrient treatments are slightly offset to show data. Regardless of nutrient status, FSC_H, Q_C and Q_N were highest at 28°C ($p<0.05$, 2-way ANOVA), supported by the positive effect of temperature on the cell shape determining protein MreB (Supplementary Figure S4; Supplementary Tables S4 and S5). Under N-stress, FSC_H, Q_C and Q_P were lowest at 24°C relative to other temperature treatments ($p<0.05$, 2-way ANOVA), supporting 24°C as T_{opt} for nutrient use. Nutrients and temperature both had significant effects on $Q_P:FSC_H$ ($p<0.05$, 2-way ANOVA), and the temperature effect was driven mostly by the difference between P-stressed cells at 20°C relative to T_{opt} (Benjamini-Hochberg, $p<0.05$), which resulted in a positive temperature effect on $C:P_{cell}$ under P-stress between 20-28°C (Benjamini-Hochberg, $p<0.05$). Nutrients and temperature significantly interact to influence $C:P_{cell}$, $C:N_{cell}$ and $Q_C:FSC_H$ ($p<0.05$, 2-way ANOVA; Supplementary Table S4).

Figure 2. Environmental drivers of cellular quotas, ratios and proteome. Portion of whole model variance of cellular elemental ratios, quotas and FSC_H (2-way ANOVA) and exclusive peak areas of all 1146 proteins (2-way PERMANOVA) attributable to $N:P_{input}$, temperature, or other effects (includes residuals and interactive effects, * denotes environmental factor has a significant influence on relative abundance, $p<0.05$). See Supplementary Tables S4 and S6 for more statistical information.

Figure 3. Consistent environmental response of abundant proteins. Clustergram representing normalized peak areas (*PA*) of the top 100 proteins in 5 replicate samples for each treatment. The clustergram function in MATLAB uses Euclidean distances in rows, correlation distances in columns and means as linkages. The sum of mean *PA* of the 100 proteins with highest *PA* (averaged across treatments) represents ~74±SE 2.5% of the cumulative sum of *PA* of all proteins measured in our analysis (% PA_{Total}; see text for explanation and Supplementary Table S5, S7 and S8 for more % PA_{Total} detail). Names of proteins in clustergram along with treatment means of % PA_{Total} are listed in

Supplementary Table S7. Bar chart indicates the observed minimum and maximum *% PA_{Total}* means with standard deviations for the 100 most-abundant proteins. *BlastP matches conserved hypothetical protein 49% with a phytase-like domain in a protein from a *Cyanobium* strain (subfamily: Synechococcoideae) and ~48% with calcium binding proteins from two other bacteria.

Figure 4. Environmental regulation of key stoichiometric traits. The percent contribution of different protein-based cell traits to the peak area of the whole observable proteome (% PA_{Total}) in 6 steady-state continuous cultures of oceanic *Synechococcus* (WH8102) under a range of temperature (20°C, 24°C and 28°C). Either N- or P-stress, is indicated with N or P, respectively ($N{:}P_{input}$ =1.7, N; $N{:}P_{input}$ =80, P). The sum of % PA_{Total} was calculated for each protein group within each sample. Boxplot represents the median of sums from 5 treatment replicate samples. Boxes indicate the 25th and 75th quartiles. Whiskers extend to the most extreme value that is not an outlier. Outliers (non-existent in these plots) are data > 1.5 times the interquartile range above or below the box. Data for subgroups (red, blue, green symbols) are means of the sum of % PA_{Total} for all proteins within the subgroup. Nutrients had the largest effects on nutrient acquisition proteins and ribosomal proteins. Temperature had the largest effects on heat shock proteins, ribosomal proteins and proteins involved in managing photosynthetic energy flow. See Supplementary Tables S6-S8 for more statistical information.

References

1. Weber TS, Deutsch C. Ocean nutrient ratios governed by plankton biogeography. *Nature* 2010; **467**: 550–554.
2. Frost PC, Benstead JP, Cross WF, Hillebrand H, Larson JH, Xenopoulos MA, et al. Threshold elemental ratios of carbon and phosphorus in aquatic consumers. *Ecol Lett* 2006; **9**: 774–779.
3. Mills MM, Arrigo KR. Magnitude of oceanic nitrogen fixation influenced by the nutrient uptake ratio of phytoplankton. *Nat Geosci* 2010; **3**: 412–416.
4. Wang W-L, Moore JK, Martiny AC, Primeau FW. Convergent estimates of marine nitrogen fixation. *Nature* 2019; **566**: 205–211.
5. Galbraith ED, Martiny AC. A simple nutrient-dependence mechanism for predicting the stoichiometry of marine ecosystems. *Proc Natl Acad Sci* 2015; **112**: 8199–8204.
6. Redfield AC, Ketchum BH, Richards FA. The influence of organisms on the composition of sea-water. In: Hill MN (ed). *The sea: ideas and observations on progress in the study of the seas. Volume 2.* 1963. John Wiley, New York, pp 26–77.
7. Martiny AC, Pham CTA, Primeau FW, Vrugt JA, Moore JK, Levin SA, et al. Strong latitudinal patterns in the elemental ratios of marine plankton and organic matter. *Nat Geosci* 2013; **6**: 279–283.
8. Teng Y-C, Primeau FW, Moore JK, Lomas MW, Martiny AC. Global-scale variations of the ratios of carbon to phosphorus in exported marine organic matter. *Nat Geosci* 2014; **7**: 895–898.

9. Tanioka T, Garcia CA, Larkin AA, Garcia NS, Fagan AJ, Martiny AC. Global patterns and predictors of C:N:P in marine ecosystems. *Commun Earth Environ 2022 31* 2022; **3**: 1–9.

10. Geider R, La Roche J. Redfield revisited: variability of C:N:P in marine microalgae and its biochemical basis. *Eur J Phycol* 2002; **37**: 1–17.

11. Moreno AR, Martiny AC. Ecological stoichiometry of ocean plankton. *Ann Rev Mar Sci* 2018; **10**: 43–69.

12. Eppley RW, Rogers JN. Inorganic nitrogen assimilation of *Ditylum brightwellii*, a marine plankton diatom. *J Phycol* 1970; **6**: 344–351.

13. Klausmeier CA, Litchman E, Daufresne T, Levin SA. Optimal nitrogen-to-phosphorus stoichiometry of phytoplankton. *Nature* 2004; **429**: 171–174.

14. Droop MR. Vitamin B_{12} and marine ecology. IV. The kinetics of uptake, growth and inhibition in *Monochrysis lutheri*. *J Mar Biol Assoc United Kingdom* 1968; **48**: 689–733.

15. Kamennaya NA, Geraki K, Scanlan DJ, Zubkov M V. Accumulation of ambient phosphate into the periplasm of marine bacteria is proton motive force dependent. *Nat Commun* 2020; **11**: 2642.

16. Martin P, Dyhrman ST, Lomas MW, Poulton NJ, Van Mooy BAS. Accumulation and enhanced cycling of polyphosphate by Sargasso Sea plankton in response to low phosphorus. *Proc Natl Acad Sci U S A* 2014; **111**: 8089–94.

17. Toseland A, Daines SJ, Clark JR, Kirkham A, Strauss J, Uhlig C, et al. The impact of temperature on marine phytoplankton resource allocation and metabolism. *Nat Clim Chang* 2013.

18. Broeze RJ, Solomon CJ, Pope DH. Effects of low temperature on *in vivo* and *in vitro*

protein synthesis in *Escherichia coli* and *Pseudomonas fluorescens*. *J Bacteriol* 1978; **134**: 861–874.

19. Klausmeier CA, Litchman E, Levin SA. Phytoplankton growth and stoichiometry under multiple nutrient limitation. *Limnol Oceanogr* 2004; **49**: 1463–1470.

20. Sterner RW, Elser JJ. Ecological stoichiometry: The biology of elements from molecules to the biosphere. 2002. Princeton University Press.

21. Bonachela JA, Allison SD, Martiny AC, Levin SA. A model for variable phytoplankton stoichiometry based on cell protein regulation. *Biogeosciences* 2013; **10**: 4341–4356.

22. Grossman AR, Schaefer MR, Chiang GG, Collier JL. Environmental effects on the light-harvesting complex of Cyanobacteria. *J Bacteriol* 1993; **175**: 575–582.

23. Güler S, Seeliger A, Härtel H, Renger G, Benning C. A null mutant of *Synechococcus* sp. PCC7942 deficient in the sulfolipid sulfoquinovosyl diacylglycerol. *J Biol Chem* 1996; **271**: 7501–7507.

24. Van Mooy BAS, Rocap G, Fredricks HF, Evans CT, Devol AH. Sulfolipids dramatically decrease phosphorus demand by picocyanobacteria in oligotrophic marine environments. *Proc Natl Acad Sci U S A* 2006; **103**: 8607–8612.

25. Van Mooy BAS, Fredricks HF, Pedler BE, Dyhrman ST, Karl DM, Koblizek M, et al. Phytoplankton in the ocean use non-phosphorus lipids in response to phosphorus scarcity. *Nature* 2009; **458**: 69–72.

26. Rao NN, Gómez-García MR, Kornberg A. Inorganic polyphosphate: essential for growth and survival. *Annu Rev Biochem* 2009; **78**: 605–647.

27. Gray M, Wholey W, Wagner N, Cremers C. Polyphosphate is a primordial chaperone. *Mol*

Cell 2014; **53**: 689–699.

28. Flombaum P, Gallegos JL, Gordillo RA, Rincón J, Zabala LL, Jiao N, et al. Present and future global distributions of the marine Cyanobacteria *Prochlorococcus* and *Synechococcus*. *Proc Natl Acad Sci U S A* 2013; **110**: 9824–9.

29. Garcia NS, Bonachela JA, Martiny AC. Interactions between growth-dependent changes in cell size, nutrient supply and cellular elemental stoichiometry of marine *Synechococcus*. *ISME J* 2016; **10**: 2715–2724.

30. Michaels A, Dow R, Elardo K. The determination of phosphorus in seawater. *Bermuda Atlantic Time Series Methods*. 1997. pp 71–74.

31. Hughes CS, Foehr S, Garfield DA, Furlong EE, Steinmetz LM, Krijgsveld J. Ultrasensitive proteome analysis using paramagnetic bead technology. *Mol Syst Biol* 2014; **10**: 757.

32. Searle BC, Pino LK, Egertson JD, Ting YS, Lawrence RT, Maclean BX, et al. Chromatogram libraries improve peptide detection and quantification by data independent acquisition mass spectrometry. *Nat Commun* 2018; **9**: 1–12.

33. Scanlan DJ, Ostrowski M, Mazard S, Dufresne A, Garczarek L, Hess WR, et al. Ecological genomics of marine picocyanobacteria. *Microbiol Mol Biol Rev* 2009; **73**: 249–299.

34. Su Z, Mao F, Dam P, Wu H, Olman V, Paulsen IT, et al. Computational inference and experimental validation of the nitrogen assimilation regulatory network in cyanobacterium *Synechococcus* sp. WH8102. *Nucleic Acids Res* 2006; **34**: 1050–1065.

35. Su Z, Olman V, Xu Y. Computational prediction of Pho regulons in Cyanobacteria. *BMC Genomics 2007 81* 2007; **8**: 1–12.

36. Tetu S, Brahamsha B, Johnson D, Tai V. Microarray analysis of phosphate regulation in

the marine Cyanobacterium *Synechococcus* sp. WH8102. *ISME J* 2009; **3**: 835–849.

37. Lee J, Müller P, Zhu Y, Ji Y. A nonparametric Bayesian model for local clustering with applications to proteomics. *J Am Stat Assoc* 2013; **108**: 775–788.

38. Sivaganesan S, Laud PW, Müller P. A Bayesian subgroup analysis with a zero-enriched Polya Urn scheme. *Stat Med* 2011; **30**: 312–323.

39. Hagen KD, Meeks JC. The unique Cyanobacterial protein OpcA is an allosteric effector of glucose-6-phosphate dehydrogenase in *Nostoc punctiforme* ATCC 29133. *J Biol Chem* 2001; **276**: 11477–11486.

40. Scanlan DJ, Sundaram S, Newman J, Mann NH, Carr NG. Characterization of a zwf mutant of *Synechococcus* sp. strain PCC 7942. *J Bacteriol* 1995; **177**: 2550–2553.

41. Zinser ER, Lindell D, Johnson ZI, Futschik ME, Steglich C, Coleman ML, et al. Choreography of the transcriptome, photophysiology, and cell cycle of a minimal photoautotroph, *Prochlorococcus*. *PLoS One* 2009; **4**: e5135.

42. Urresti S, Albesa-Jove D, Schaeffer F, Pham HT, Kaur D, Gest P, et al. Mechanistic insights into the retaining glucosyl-3-phosphoglycerate synthase from Mycobacteria. *J Biol Chem* 2012; **287**: 24649–24661.

43. Klähn S, Steglich C, Hess WR, Hagemann M. Glucosylglycerate: A secondary compatible solute common to marine Cyanobacteria from nitrogen-poor environments. *Environ Microbiol* 2010; **12**: 83–94.

44. Snyder DS, Brahamsha B, Azadi P, Palenik B. Structure of compositionally simple lipopolysaccharide from marine *Synechococcus*. *J Bacteriol* 2009; **191**: 5499–5509.

45. Park JT, Uehara T. How bacteria consume their own exoskeletons (turnover and recycling

of cell wall peptidoglycan). *Microbiol Mol Biol Rev* 2008; **72**: 211–227.

46. Mouginot C, Zimmerman AE, Bonachela JA, Fredricks H, Allison SD, Van Mooy BAS, et al. Resource allocation by the marine cyanobacterium *Synechococcus* WH8102 in response to different nutrient supply ratios. *Limnol Oceanogr* 2015; **60**: 1634–1641.

47. Piven I, Ajlani G, Sokolenko A. Phycobilisome linker proteins are phosphorylated in *Synechocystis* sp. PCC 6803. *J Biol Chem* 2005; **280**: 21667–21672.

48. Garcia CA, Hagstrom GI, Larkin AA, Ustick LJ, Levin SA, Lomas MW, et al. Linking regional shifts in microbial genome adaptation with surface ocean biogeochemistry. *Philos Trans R Soc B Biol Sci* 2020; **375**.

49. Garcia NS, Talmy D, Fu W-W, Larkin AA, Lee J, Martiny AC. The diel cycle of surface ocean elemental stoichiometry has implications for ocean productivity. *Global Biogeochem Cycles* 2022; **36**: e2021GB007092.

50. Rhee GY. Effects of N:P atomic ratios and nitrate limitation on algal growth, cell composition, and nitrate uptake. *Limnol Oceanogr* 1978; **23**: 10–25.

51. Nagata T, Watanabe Y. Carbon- and nitrogen-to-volume ratios of bacterioplankton grown under different nutritional conditions. *Appl Environ Microbiol* 1990; **56**: 1303–1309.

52. Montagnes DJS, Berges JA, Harrison PJ, Taylor FJR. Estimating carbon, nitrogen, protein, and chlorophyll a from volume in marine phytoplankton. *Limnol Oceanogr* 1994; **39**: 1044–1060.

53. Warr SRC, Reed RH, Stewart WDP. Carbohydrate accumulation in osmotically stressed Cyanobacteria (blue-green algae): interactions of temperature and salinity. *New Phytol* 1985; **100**: 285–292.

54. Hickman J, Kotovic K, Miller C, Warrener P. Glycogen synthesis is a required component of the nitrogen stress response in *Synechococcus elongatus* PCC 7942. *Algal Res* 2013; **2**: 98–106.

55. Mullineaux CW, Tobin MJ, Jones GR. Mobility of photosynthetic complexes in thylakoid membranes. *Nature* 1997; **390**: 421–424.

56. Cox AD, Saito MA, Basu P, Boyd E, Pacheco LGC. Proteomic responses of oceanic *Synechococcus* WH8102 to phosphate and zinc scarcity and cadmium additions. *Front Microbiol* 2013; **4**.

57. Giovannoni SJ, Cameron Thrash J, Temperton B. Implications of streamlining theory for microbial ecology. *ISME J* 2014; **8**: 1553–1565.

58. Mackey KRM, Paytan A, Caldeira K, Grossman AR, Moran D, McIlvin M, et al. Effect of temperature on photosynthesis and growth in marine *Synechococcus* spp. *Plant Physiol* 2013; **163**: 815–29.

59. Varkey D, Mazard S, Ostrowski M, Tetu SG, Haynes P, Paulsen IT. Effects of low temperature on tropical and temperate isolates of marine *Synechococcus*. *ISME J 2016 105* 2015; **10**: 1252–1263.

60. Sato M, Nimura-Matsune K, Watanabe S, Chibazakura T, Yoshikawa H. Expression analysis of multiple dnaK genes in the Cyanobacterium *Synechococcus elongatus* PCC 7942. *J Bacteriol* 2007; **189**: 3751–3758.

61. Shi H, Bratton BP, Gitai Z, Huang KC. How to build a bacterial cell: MreB as the foreman of *E. coli* construction. *Cell* 2018; **172**: 1294–1305.

62. Forster J, Hirst AG, Esteban GF. Achieving temperature-size changes in a unicellular

organism. *ISME J* 2013; **7**: 28–36.

63. Ustick LJ, Larkin AA, Garcia CA, Garcia NS, Brock ML, Lee JA, et al. Metagenomic analysis reveals global-scale patterns of ocean nutrient limitation. *Science (80-)* 2021; **372**: 287–291.

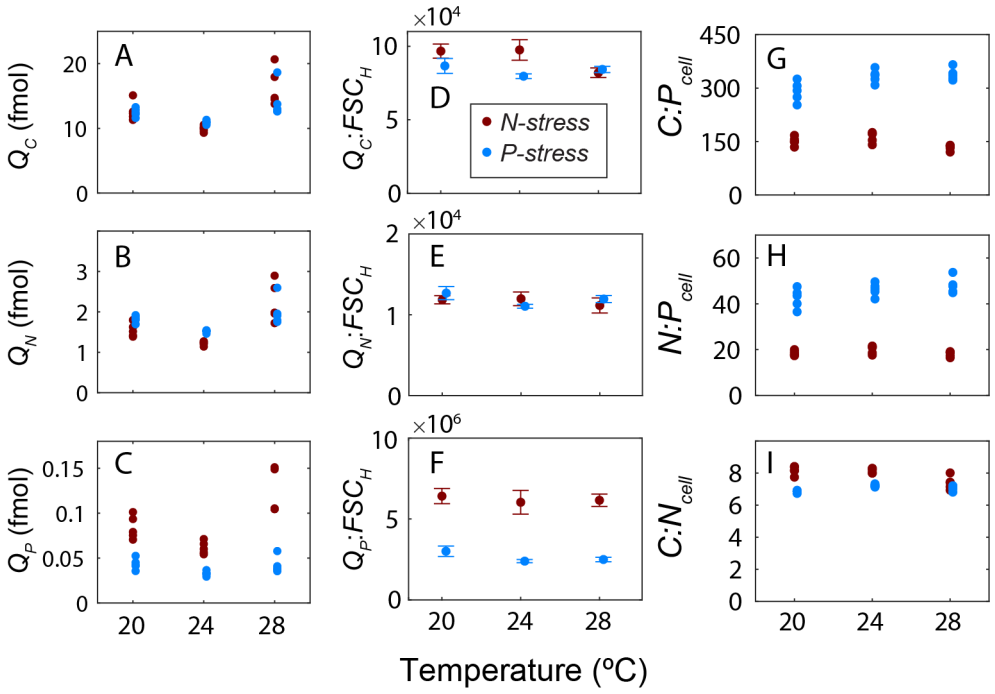
A
B
C
D
E
F
G
H
I
Q_C (fmol)
Q_N (fmol)
Q_P (fmol)
Q_C:FSC_H
Q_N:FSC_H
Q_P:FSC_H
C:P_{cell}
N:P_{cell}
C:N_{cell}
×10^4
×10^4
×10^6
N-stress
P-stress
Temperature (°C)
20
24
28

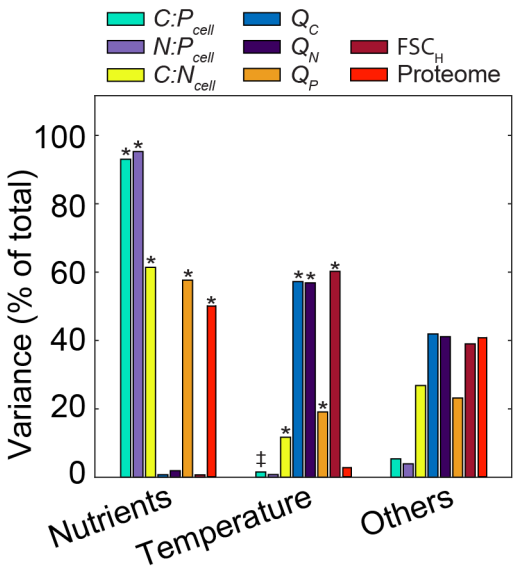
C:P cell
N:P cell
C:N cell
Q C
Q N
Q P
FSC H
Proteome
Variance (% of total)
100
80
60
40
20
0
Nutrients
Temperature
Others

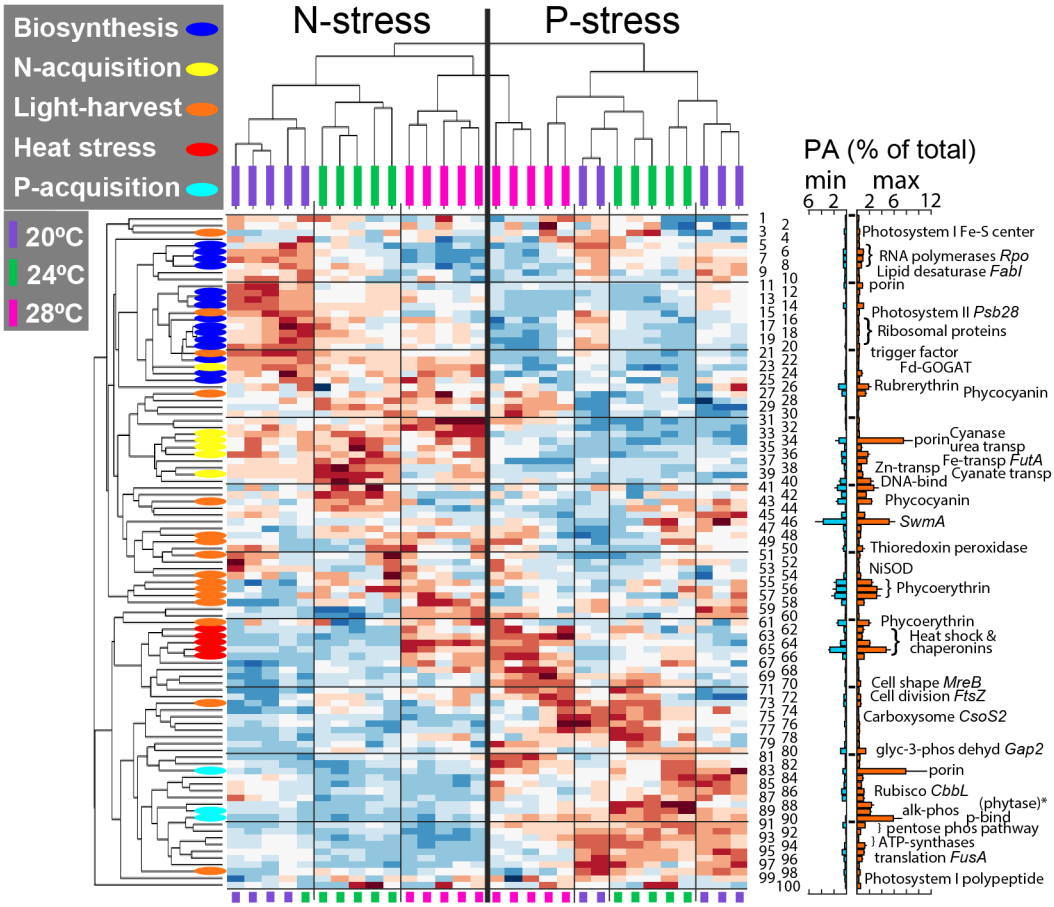
Biosynthesis
N-acquisition
Light-harvest
Heat stress
P-acquisition
20ºC
24ºC
28ºC
N-stress
P-stress
PA (% of total)
min max
6 2
2 6 12
Photosystem I Fe-S center
RNA polymerases Rpo
Lipid desaturase FabI
porin
Photosystem II Psb28
Ribosomal proteins
trigger factor
Fd-GOGAT
Rubrerythrin
Phycocyanin
porin
Cyanase
urea transp
Fe-transp FutA
Zn-transp
Cyanate transp
DNA-bind
Phycocyanin
SwmA
Thioredoxin peroxidase
NiSOD
Phycoerythrin
Phycoerythrin
Heat shock & chaperonins
Cell shape MreB
Cell division FtsZ
Carboxysome CsoS2
glyc-3-phos dehyd Gap2
porin
Rubisco CbbL
alk-phos
(phytase)*
p-bind
pentose phos pathway
ATP-synthases
translation FusA
Photosystem I polypeptide

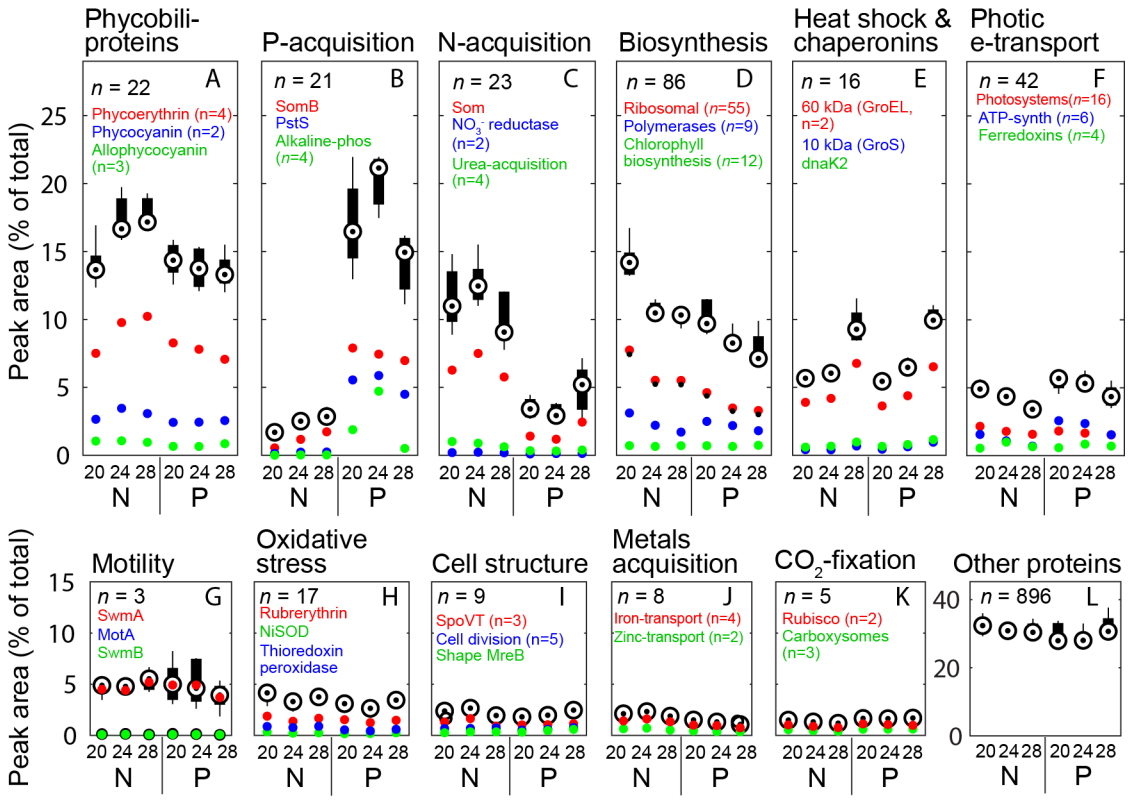
Phycobili-proteins
n = 22
A
Phycoerythrin (n=4)
Phycocyanin (n=2)
Allophycocyanin (n=3)
P-acquisition
n = 21
B
SomB
PstS
Alkaline-phos (n=4)
N-acquisition
n = 23
C
Som
NO3- reductase (n=2)
Urea-acquisition (n=4)
Biosynthesis
n = 86
D
Ribosomal (n=55)
Polymerases (n=9)
Chlorophyll biosynthesis (n=12)
Heat shock & chaperonins
n = 16
E
60 kDa (GroEL, n=2)
10 kDa (GroS)
dnaK2
Photic e-transport
n = 42
F
Photosystems(n=16)
ATP-synth (n=6)
Ferredoxins (n=4)
Peak area (% of total)
0
5
10
15
20
25
20 24 28 20 24 28
N
P
Motility
n = 3
G
SwmA
MotA
SwmB
Oxidative stress
n = 17
H
Rubrerythrin
NiSOD
Thioredoxin peroxidase
Cell structure
n = 9
I
SpoVT (n=3)
Cell division (n=5)
Shape MreB
Metals acquisition
n = 8
J
Iron-transport (n=4)
Zinc-transport (n=2)
CO2-fixation
n = 5
K
Rubisco (n=2)
Carboxysomes (n=3)
Other proteins
n = 896
L
0
5
10
15
20
40